

# RESEARCH MEMORANDUM

INTERNAL FLOW AND BURNING CHARACTERISTICS OF 16-INCH  
RAM JET OPERATING IN A FREE JET AT MACH NUMBERS  
OF 1.35 AND 1.73

By Eugene Perchonok and John M. Farley

Lewis Flight Propulsion Laboratory  
Cleveland, Ohio

NATIONAL ADVISORY COMMITTEE  
FOR AERONAUTICS  
WASHINGTON

May 21, 1951  
Declassified April 15, 1958



## NATIONAL ADVISORY COMMITTEE FOR AERONAUTICS

RESEARCH MEMORANDUM

## INTERNAL FLOW AND BURNING CHARACTERISTICS OF 16-INCH

## RAM JET OPERATING IN A FREE JET AT MACH NUMBERS

OF 1.35 and 1.73

By Eugene Perchonok and John M. Farley

## SUMMARY

A free-jet investigation of the internal-flow and burning characteristics of a 16-inch ram jet was conducted in the NACA Lewis altitude wind tunnel. Data were obtained at Mach numbers of 1.35 and 1.73 over a range of exit-nozzle areas. A single oblique shock diffuser with no internal contraction and a corrugated gutter-grid flame holder were employed. At both Mach numbers, the inlet spike was positioned to allow the conical nose shock to intersect the cowl lip.

Excellent agreement was observed between the cold-flow and burning diffuser total-pressure recovery under both subcritical and supercritical operation. The trends in the variation of additive drag and the normal-shock position with mass-flow ratio agreed with those theoretically predicted. The total-pressure drop across the combustion chamber could be predicted with reasonable accuracy from the computed flame-holder and combustion momentum pressure losses.

At any combustion-chamber-inlet Mach number, either subcritical or supercritical, similar velocity distributions resulted at the combustion-chamber inlet for both the present free-jet investigation and a previously conducted connected-pipe investigation. As a result, combustion-chamber performance was obtained in the free jet similar to that previously obtained with a connected pipe.

## INTRODUCTION

As part of a general program to evaluate the performance potentialities of the ram jet as a supersonic power plant, connected-pipe and free-jet investigations of a 16-inch ram jet were made in the NACA Lewis altitude wind tunnel. The connected-pipe performance of this engine with several different combustion-chamber configurations is reported in reference 1. Free-jet performance with two of

the same combustion-chamber configurations and the effect of several fuels on engine performance, obtained with a third combustion chamber configuration, have also been reported (references 2 and 3). No supercritical performance data, however, are presented.

A more complete engine-performance evaluation, including an analysis of the internal-flow and burning characteristics at zero angle of attack, with the third combustion-chamber configuration is now available and is presented herein. The effects of operating conditions on diffuser pressure recovery, additive drag, velocity and static-pressure distribution in the subsonic diffuser, and change in internal engine performance with variation in exit-nozzle area are considered at Mach numbers of 1.35 and 1.73 and altitudes of 35,000 and 41,000 feet, respectively.

#### APPARATUS

A description of the altitude-wind-tunnel facility and the 16-inch ram jet with which this investigation was made is given in reference 2. A schematic drawing of the engine is presented in figure 1 and the engine coordinates are given in table I. Two free-jet nozzles, each having a 12-inch-diameter discharge and operating Mach numbers of 1.35 and 1.73, respectively, were used in this investigation.

A single oblique shock inlet designed for external compression was used. The spike-tip projection was remotely adjustable and was positioned at each stream Mach number to cause the oblique shock generated by the cone to intercept the inlet lip. The diffuser-inlet lip had a 0.004-inch radius and its outer surface was at  $11^\circ$  to the horizontal. A remotely adjustable tail plug permitted an exit-nozzle-area variation from 51 to 74 percent of the combustion-chamber area, with the minimum flow area at the nozzle exit for all plug positions.

The fuel-injection plane was 74 inches downstream of the inlet lip, and the fuel was sprayed in an upstream direction. The fuel injector (fig. 2) consisted of four dual-arc segments each of which held four commercial spray nozzles modified to reduce their frontal area. The fuel used in this investigation was a clear, unleaded gasoline having the designation AN-F-48B, grade 80. Propylene oxide was used as a fuel in the vortex-type pilot burner.

The flame holder used in this investigation (fig. 3) was located 17 inches downstream of the fuel injector. It consisted of a series of corrugated gutters having a chord of 2 inches, a spacing of 1 inch between corrugations, and an angular gutter variation from  $35^\circ$  to  $53^\circ$  included angle. Smaller uncorrugated connecting gutters were welded between the corrugated sections. The flame holder was mounted with the inner rim around the pilot-burner exit and blocked 54 percent of the annular area. The cold-flow flame-holder pressure-drop coefficient, including the combustion-chamber cold-flow friction loss, is presented in reference 1 and is reproduced in figure 4.

The air flow through the engine was calculated from a total- and static-pressure survey made 62 inches downstream of the inlet lip, station x. Additional total-pressure surveys were made at stations y and z. (See fig. 1.) Traces of the static-pressure fluctuations at station x were obtained with a commercial strain-gage-type pressure pickup. Engine thrust and exhaust-gas temperatures were calculated by the methods of references 4 and 5 from pressure measurements made with rakes mounted at the nozzle outlet. Static wall orifices were placed along the length of the entire engine. Similar orifices were used to obtain wall pressures on the centerbody and the projecting spike.

A shadowgraph system was employed in studying the air-flow pattern about the engine inlet.

#### SYMBOLS

The following symbols are used in this report:

A	cross-sectional area, (sq ft)
$C_{D,a}$	additive drag coefficient (based on inlet area)
$C_F$	net-internal-thrust coefficient, $\frac{2F_n}{\gamma_0 p_0 A_4 M_0^2}$
$F_n$	net-internal thrust, (lb)
f/a	fuel-air ratio
K	constant
L/Y	ratio between distance of normal shock wave ahead of diffuser inlet to diffuser-inlet diameter

M	Mach number
$m/m_0$	mass-flow ratio, ratio of actual air-mass flow through engine to mass flow contained in free-stream tube having diameter equal to diffuser-inlet diameter
P	total pressure, (lb/sq ft absolute)
p	static pressure, (lb/sq ft absolute)
q	dynamic pressure, (lb/sq ft absolute)
T	total temperature, °R
t	static temperature, °R
$W_a$	air flow, (lb/sec)
$\delta_0$	ratio of test-section ambient pressure to absolute static pressure of NACA standard atmosphere at sea level, $p_0/2116$
$\gamma$	ratio of specific heat at constant pressure to specific heat at constant volume
$\theta_0$	ratio of static temperature of free jet to NACA standard temperature at sea level, $t_0/519$
$\eta_b$	combustion efficiency, percent
$\tau$	ratio of absolute total temperature at exhaust-nozzle outlet to absolute total temperature at combustion-chamber inlet
tsfc	thrust specific fuel consumption, (lb fuel/hr/lb thrust)

Subscripts (refer to fig. 1):

0	free-stream condition
1	supersonic-diffuser inlet
2	subsonic-diffuser inlet (by definition)
3	diffuser outlet and combustion-chamber inlet

4	combustion chamber
5	combustion-chamber outlet
6	nozzle outlet
x	station 62 inches downstream of inlet lip
y	station 12 inches downstream of inlet lip
z	station 84 inches downstream of inlet lip

## RESULTS AND DISCUSSION

Because the inlet spike was positioned to allow the conical nose shock to intersect the cowl lip at both Mach numbers investigated, the results obtained represent on-design performance at both  $M_0 = 1.35$  and 1.73.

### Diffuser Performance

Variation of the static-wall pressure coefficients in the region of the engine inlet at  $M_0 = 1.73$  are presented in figure 5 for both cold-flow and burning conditions. For subcritical flow ( $M_3 < 0.195$ ), excellent agreement between the wall-static-pressure distribution for cold-flow and burning conditions is observed. Supercritically, however, only moderate agreement is noted and may possibly be a result of small differences in  $M_3$  between the two cases.

The occurrence of the normal shock is characterized by a rise in static pressure. Subcritically, the rise, occurring externally on the spike, is abrupt. At  $M_3 = 0.22$ , the normal shock occurs in a region from 1 to 2 inches inside of the cowl lip and may also be considered abrupt. The rise in wall pressure due to the normal shock, however, was followed by an unexplained dip in wall pressure sufficient to accelerate considerably the flow in this region. Because a similar dip occurred for subcritical flow, the wall-static-pressure distribution in this region cannot be considered part of the normal-shock structure. It is believed that this phenomenon was characteristic of the particular engine configuration and probably causes a measurable diffuser pressure loss.

Some difference exists in wall-static pressure between the center body and the outer shell in the first few inches downstream of the lip. At the next point of comparison, 11 inches downstream of the lip, however, identical values were obtained, and from this point to the combustion-chamber inlet essentially constant static pressures across the duct were noted at all stations.

Diffuser pressure recovery. - The over-all and subsonic-diffuser total-pressure recoveries at stream Mach numbers of 1.73 and 1.35 are presented in figure 6 for both cold-flow and burning conditions. Because previous calibration of the free-jet nozzles indicated a negligible loss in total pressure across the nozzle, the over-all diffuser pressure recovery was calculated from total-pressure measurements at the nozzle inlet and station  $x$  in the diffuser. By definition, the subsonic-diffuser pressure recovery is taken as the ratio of total pressures between stations  $x$  and  $y$ .

Good agreement was obtained between cold-flow and burning conditions for the over-all diffuser total-pressure recovery as well as for the subsonic-diffuser pressure recovery. The subcritical "pulsing" encountered under both cold-flow and burning conditions was of such low magnitude that the diffuser pressure recovery was not seriously affected. Over the mass-flow range investigated at both Mach numbers, the over-all subcritical pressure recovery varied only slightly. At  $M_0 = 1.73$ , the average subcritical pressure recovery was  $88 \pm 1$  percent and at  $M_0 = 1.35$  approximately  $97 \pm 1$  percent.

At both Mach numbers, the critical pressure recovery was less than the theoretical maximum value. The subsonic-diffuser total-pressure loss, which amounted to about 2 percent and remained relatively constant and independent of stream Mach number, accounts for part of this difference. The remaining discrepancy may be due, in part, to the flow disturbances observed downstream of the cowl lip.

Additive drag. - The variation with mass-flow ratio of the additive drag coefficient (based on cowl-inlet area) is presented in figure 7. The experimental values were calculated from a momentum balance based on pressures, measured at station  $y$  and on the spike. The data graphically show the large drag penalty of subcritical-diffuser operation, even at Mach numbers as low as 1.35. Both the increase in  $C_{D,a}$  with  $M_0$  and, at a given  $M_0$ , the essentially linear increase in  $C_{D,a}$  as the engine air flow is reduced verify the trends predicted by reference 6.

Effect of mass-air flow on normal-shock position. - A shadowgraph of the engine inlet for the most severe pulsing condition encountered while burning ( $M_0 = 1.73$ ,  $M_3 = 0.17$ ) is shown in figure 8(a). The extremes of the normal-shock positions are clearly defined. A shadowgraph of the inlet at the same Mach number under cold-flow conditions is shown in figure 8(b). The corresponding diffuser-exit static-pressure traces are also shown.

In general, at a given mass-air flow the cold-flow normal-shock movement was essentially sinusoidal and of negligible amplitude. It is therefore possible to assign a mean-shock position and from the shadowgraph image obtain a curve giving the variation in normal-shock position with mass-flow ratio (fig. 9). Shock positions are presented nondimensionally in terms of the diffuser-inlet diameter and the data scatter somewhat. Below a mass-flow ratio of 0.9, the variation of shock position with mass-flow ratio is essentially linear. The theoretical variation predicted in reference 7 confirms this trend but for a given shock position predicts a lower air flow than actually obtained. Although it is admittedly difficult to experimentally evaluate the mass-flow ratio, this difference could well be associated with the approximations in the theory. As the mass-flow ratio is raised from 0.9 to 1.0, the spread between the experimental data and the theoretical curve decreases.

The instantaneous shock position under severe pulsing conditions, determined from shadowgraph high-speed motion pictures, was integrated over a reasonable time interval to determine an average normal-shock position. The value of the mass-flow ratio from figure 9 corresponding to the average-shock position so determined agreed with the value determined from pressure instrumentation at station x. It thus appears that for the diffuser configuration investigated, the mass flows determined from pressure instrumentation under severe pulsing conditions represent a valid time-average mass flow, and in the absence of such instrumentation the mass flow can be determined from an integration of the normal-shock movement.

Air flow. - The diffuser air-flow characteristics are presented as a function of combustion-chamber-inlet Mach number  $M_3$  in figure 10 in terms of the generalized air-flow parameter. This parameter is derived from the continuity of mass flow through the diffuser and at a constant  $M_0$  is given by the following expression:

$$\frac{W_a \sqrt{\theta_0}}{\delta_0} = K \left( \frac{P_3}{P_0} \right) \left[ \frac{M_3}{\left( 1 + \frac{\gamma-1}{2} M_3^2 \right)^{\frac{\gamma+1}{2(\gamma-1)}}} \right]$$

The actual value of the parameter, as plotted, represents the engine air flow reduced to standard sea-level conditions and is therefore independent of the ambient pressure and temperature. Thus for a given  $M_0$ , the air flow at any altitude and  $M_3$  can be determined from a single curve. For this particular diffuser configuration, the subcritical mass flow increases linearly with  $M_3$ . Below

combustion-chamber-inlet Mach numbers of 0.3, the function of  $M_3$  in the equation increases linearly with  $M_3$ ; and because the subcritical-diffuser pressure recovery varies so little, the subcritical mass flow for this configuration could be approximated quite accurately by a straight line joining the origin and the critical-flow condition.

Velocity and pressure distribution. - The Mach number distributions for  $M_0 = 1.73$  at stations 12, 62, and 84 inches downstream of the inlet lip are given in figure 11. Free-jet data are presented over a range of combustion-chamber-inlet Mach numbers, including both subcritical- and supercritical-diffuser operation, under cold-flow as well as burning conditions. In addition, connected-pipe-burning data (reference 1) for the same  $M_3$  conditions are also presented.

It is apparent from the free-jet data that the velocity profile is not symmetrical either circumferentially or across the annulus; and although the velocity distribution changed markedly with combustion-chamber-inlet Mach number, agreement between the free-jet cold-flow and burning profiles was observed. The asymmetry in profile is most apparent near the diffuser inlet. For example, at supercritical conditions the air flow in the region of station y (fig. 11(a)) tends to concentrate toward the outer shell; whereas under subcritical conditions the velocity peak shifts toward the inner body. A similar trend is evident but to a lesser degree at station x (fig. 11(b)), and at station z (fig. 11(c)) the shift is negligible. Although the origin of the circumferential asymmetry at station x could not be determined, it is believed to arise within the engine itself inasmuch as a survey of the free jet indicated symmetrical flow in the region of the engine inlet.

It is interesting to note for the case of the connected pipe that due to the development of fully turbulent flow in the approach duct to the engine inlet, a flat uniform velocity distribution is obtained at station y. Also, at a given diffuser-outlet Mach number, either subcritical or supercritical, similar velocity distributions resulted at station z for both connected-pipe and free-jet burning operation. If it can be assumed that essentially similar velocity distributions also exist in the region of the fuel injector as well, valid combustion-chamber-performance evaluation should result with connected-pipe operation.

## Combustion-Chamber Performance

Curves showing the effect of exit-nozzle area and fuel-air ratio on combustion-chamber performance are presented in figure 12 for  $M_0 = 1.73$  at 41,000 feet and  $M_0 = 1.35$  at 35,000 feet. In each case the inlet-air total temperature was set in accordance with the NACA standard atmosphere.

As calculated, the exhaust-gas temperature does not include the heat released by the fuel and rejected to the water used in cooling the tail plug and the combustion chamber. If the energy absorbed by the cooling water is added to the exhaust gases, an increase from  $50^\circ$  to  $200^\circ$  F in the values of the exhaust-gas temperatures reported herein would result. This change would be reflected as an increase in the total-temperature ratio  $\tau$  across the engine. In the evaluation of the combustion efficiency  $\eta_b$ , however, both the energy content of the pilot fuel as well as the energy given up to the cooling water were considered.

Lean blow-out appears uninfluenced by the difference in combustion-chamber-inlet pressure and temperature between the two Mach numbers; however, rich blow-out appears extended somewhat by an increase in combustion-chamber-inlet static pressure and temperature. The fuel-air-ratio range was fairly large at both stream Mach numbers and rich blow-out occurred in the region of maximum combustion efficiency but below the stoichiometric fuel-air ratio. Although at a given fuel-air ratio the combustion-chamber-inlet Mach number  $M_3$  (based on the annular area at station 3) decreased as the outlet area was reduced, the combustion efficiency was not necessarily maximum at the smallest outlet area.

Combustion efficiencies in the order of 70 percent were obtained from fuel-air ratios of 0.035 to 0.053 at  $M_0 = 1.73$  and an outlet-area ratio of 0.676. The corresponding  $M_3$  range was 0.195 to 0.173. The combustion efficiencies at the other outlet-area ratios were also relatively flat in this fuel-air ratio region, and in general at a given fuel-air ratio the spread in combustion efficiency as a result of outlet-area changes was only 10 percent. At  $M_0 = 1.73$ , the values of the total-temperature ratio across the combustion chamber  $\tau$  ranged between 1.9 and 4.6, whereas at  $M_0 = 1.35$  due to the reduced fuel-air ratio range and lower inlet-air temperatures the  $\tau$  value varied between 2.3 and 4.7.

The connected-pipe performance of this same combustion-chamber configuration with the identical fuel-injector radius setting, 5.22 inches, is presented in reference 1 and is reproduced in figure 12(a). Essentially the same operable fuel-air-ratio range and the same level of combustion efficiencies as obtained in the free jet are indicated. Although some diffuser pulsing was present there was no noticeable change in combustion-chamber operation between subcritical and supercritical conditions. Both of these results are valid only for the configuration investigated and were expected on the basis of the similarities in diffuser-outlet velocity distribution.

The effect of  $\tau$  and  $M_3$  on the total-pressure ratio across the combustion chamber (combined flame-holder and combustion momentum losses) is shown in figure 13. The theoretical curves were derived by combining the actual flame-holder losses (fig. 4) with the one-dimensional frictionless combustion momentum losses. Good agreement in trend and magnitude is obtained between the experimental and the theoretical values, even though fluid viscosity was neglected. It may be concluded that for analytical purposes the constant-area combustion-chamber total-pressure drop can be estimated on a one-dimensional frictionless basis with reasonable accuracy.

Also shown on figure 13 is the experimental variation in total-pressure ratio across the combustion chamber with  $M_3$  at  $M_0 = 1.73$  for several exit-nozzle areas. The increased loss in pressure as  $M_3$  is raised results from the presence of the flame holder rather than an increased combustion momentum drop and is less severe with flame holders having lower flow losses.

#### Engine Performance

The effects of  $\tau$  and exit-nozzle area on the net internal thrust coefficient (based on combustion-chamber area) and the specific fuel consumption in pounds per hour per pound of thrust are presented in figure 14. As has often been demonstrated with a fixed-outlet area, the internal thrust coefficient  $C_F$  increases with  $\tau$ ; however, at a fixed  $\tau$ ,  $C_F$  does not always increase with outlet area. For example at  $M_0 = 1.35$ , essentially a single curve describes the variation of internal thrust with  $\tau$  for all outlet areas (fig. 14(b)). On the other hand at  $M_0 = 1.73$ , the thrust coefficient increases with outlet area for all values of  $\tau$  above 3.5. Below this value of  $\tau$ , the area curves cross and result in greater internal thrust coefficients at outlet areas less than

the maximum investigated. This apparent inconsistency arises from the interrelation of mass air flow, diffuser pressure recovery, and combustion-chamber pressure losses. It would appear by extrapolation that a value of  $\tau$  of at least 1.5 is required to overcome the internal-flow losses at both stream Mach numbers.

The thrust-specific-fuel-consumption trends are markedly influenced by the combustion efficiency, which masks the general effect of  $\tau$  and exit area on thrust specific fuel consumption. Although the data indicate a rapid reduction in thrust specific fuel consumption as  $\tau$  is raised from 2 to 3, the rate of reduction in the value of thrust specific fuel consumption as  $\tau$  is increased beyond 3 drops considerably. At  $M_0 = 1.73$ , an essentially constant thrust specific fuel consumption was observed between  $\tau = 3.3$  and 4.5 for a given exit-nozzle area (fig. 14(a)). The minimum fuel consumption were 3.0 and 3.8 pounds of fuel per hour per pound of thrust at  $M_0 = 1.73$  and 1.35, respectively.

In order to better illustrate the effect of  $\tau$  and exit-area ratio on the fuel consumption, the data have been generalized to 100-percent combustion efficiency, thus eliminating that variable from consideration (fig. 15). This parameter indicates trends at a constant  $\eta_b$ , and although it represents the actual fuel consumption at an  $\eta_b$  of 100 percent, the parameter can be used to evaluate the fuel consumption at any combustion efficiency. Large reductions in the fuel consumption result from improved combustion efficiency. For example, at  $M_0 = 1.35$  and 1.73 the minimum fuel consumption can be reduced to 2.46 and 1.86 pounds per hour per pound, respectively, if combustion efficiencies of 100 percent be attained.

As expected on the basis of the combustion-chamber pressure losses, the minimum value of the specific-fuel-consumption parameter decreased with exit area. Moreover, for all outlet areas investigated at both Mach numbers, this minimum value occurred at combustion-chamber-inlet Mach numbers between 0.195 and 0.200. It is coincidental that at  $M_0 = 1.73$  the critical  $M_3$  falls in this region. For values of  $\tau$  other than that corresponding to the minimum value, the fuel-consumption-parameter increase rapidly.

#### SUMMARY OF RESULTS

A free-jet investigation was made of the internal-flow and burning characteristics of a 16-inch ram jet employing an external compression inlet, a variable-area outlet, and a corrugated gutter-

grid flame holder. Engine performance was determined at  $M_0 = 1.73$  and  $1.35$ . The spike tip projection was adjustable and at both Mach numbers the inlet spike was positioned to allow the conical nose shock to intersect the cowl lip. The following results were obtained:

1. Excellent agreement was observed between the combined subsonic- and supersonic-diffuser total-pressure recovery for cold-flow and burning conditions under both subcritical and supercritical operation.
2. The trends in the measured additive drag agreed with that theoretically predicted. At a given mass-flow ratio the additive drag increased with  $M_0$ , and at a given  $M_0$  the additive drag increased rapidly and essentially linearly as the mass-flow ratio was reduced.
3. The variation of the normal-shock position with mass-flow ratio agreed with the trend theoretically predicted. For a given normal-shock position, however, the theory predicted a lower air flow than actually obtained.
4. Although there was a considerable radial shift in the peak local velocity at the engine inlet between subcritical and supercritical conditions, similar velocity distributions resulted at the combustion-chamber inlet for both connected-pipe and free-jet burning operation. As a result, combustion-chamber operation similar to that observed with a connected pipe was obtained in the free jet.
5. The total-pressure drop across the combustion chamber can be predicted with reasonable accuracy on the basis of the cold-flow flame-holder pressure-drop coefficient and the combustion momentum loss computed from one-dimensional frictionless-flow considerations.
6. The general level of the maximum combustion efficiencies was in the order of 70 percent and combustion-chamber temperature-ratio values between 1.9 and 4.7 were obtained. Minimum fuel consumptions of 3.8 and 3.0 pounds per hour per pound of thrust were noted at  $M_0 = 1.35$  and  $1.73$ , respectively.

Lewis Flight Propulsion Laboratory,  
National Advisory Committee for Aeronautics,  
Cleveland, Ohio.

2136

## REFERENCES

1. Nussdorfer, T. J., Sederstrom, D. C., and Perchonok, E.: Investigation of Combustion in 16-Inch Ram Jet under Simulated Conditions of High Altitude and High Mach Number. NACA RM E50D04, 1950.
2. Wilcox, Fred, Baker, Sol, and Perchonok, Eugene: Free-Jet Investigation of a 16-Inch Ram Jet at Mach Numbers of 1.35, 1.50, and 1.73. NACA RM E50G19, 1950.
3. Wilcox, Fred A.: Free-Jet Performance of 16-Inch Ram-Jet Engine with Several Fuels. NACA RM E50I06, 1950.
4. Perchonok, Eugene, Sterbentz, William H., and Wilcox, Fred A.: Performance of a 20-Inch Steady-Flow Ram Jet at High Altitudes and Ram-Pressure Ratios. NACA RM E6L06, 1947.
5. Perchonok, Eugene, Wilcox, Fred A., and Sterbentz, William H.: Preliminary Development and Performance Investigation of a 20-Inch Steady-Flow Ram Jet. NACA ACR E6D05, 1946.
6. Sibulkin, Merwin: Theoretical and Experimental Investigation of Additive Drag. NACA RM E51B13, 1951.
7. Moeckel, W. E.: Approximate Method for Predicting Form and Location of Detached Shock Waves Ahead of Plane or Axially Symmetric Bodies. NACA TN 1921, 1949.

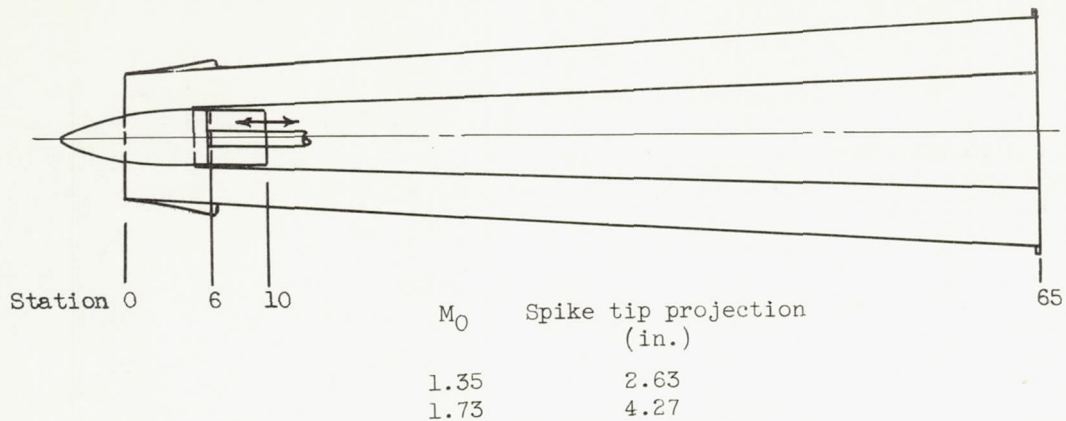


TABLE I - COORDINATES OF 16-INCH RAM JET

Shell		Diffuser inner-body coordinates		Spike coordinates	
Station (in.)	Inside diameter (in.)	Station (in.)	Outside diameter (in.)	Distance from apex (in.)	Outside diameter (in.)
0	9.00	$4\frac{3}{4}$	4.00	0 to 3	$46^\circ$ cone
0 to 1	$16^\circ$ cone	$5\frac{3}{4}$	4.16	$3\frac{1}{2}$	2.94
1	9.28	6	4.19	$3\frac{3}{4}$	3.16
$1\frac{1}{2}$	9.36	$6\frac{1}{4}$	4.22	4	3.34
2	9.44	$6\frac{1}{2}$	4.25	$4\frac{1}{4}$	3.50
$2\frac{1}{2}$	9.52	$6\frac{3}{4}$	4.28	$4\frac{1}{2}$	3.64
3	9.60	$9\frac{3}{4}$	4.56	$4\frac{3}{4}$	3.72
$3\frac{1}{2}$	9.66	10	4.56	5	3.82
4	9.72	65	8.00	$5\frac{1}{4}$	3.88
$4\frac{1}{2}$	9.76	75	8.00	$5\frac{1}{2}$	3.92
5	9.82	91	6.00	$5\frac{3}{4}$	3.94
6	9.92			$6\frac{1}{4}$	3.98
65 to 172	16.00			$6\frac{1}{2}$ to $9\frac{3}{4}$	4.00
181	13.75				

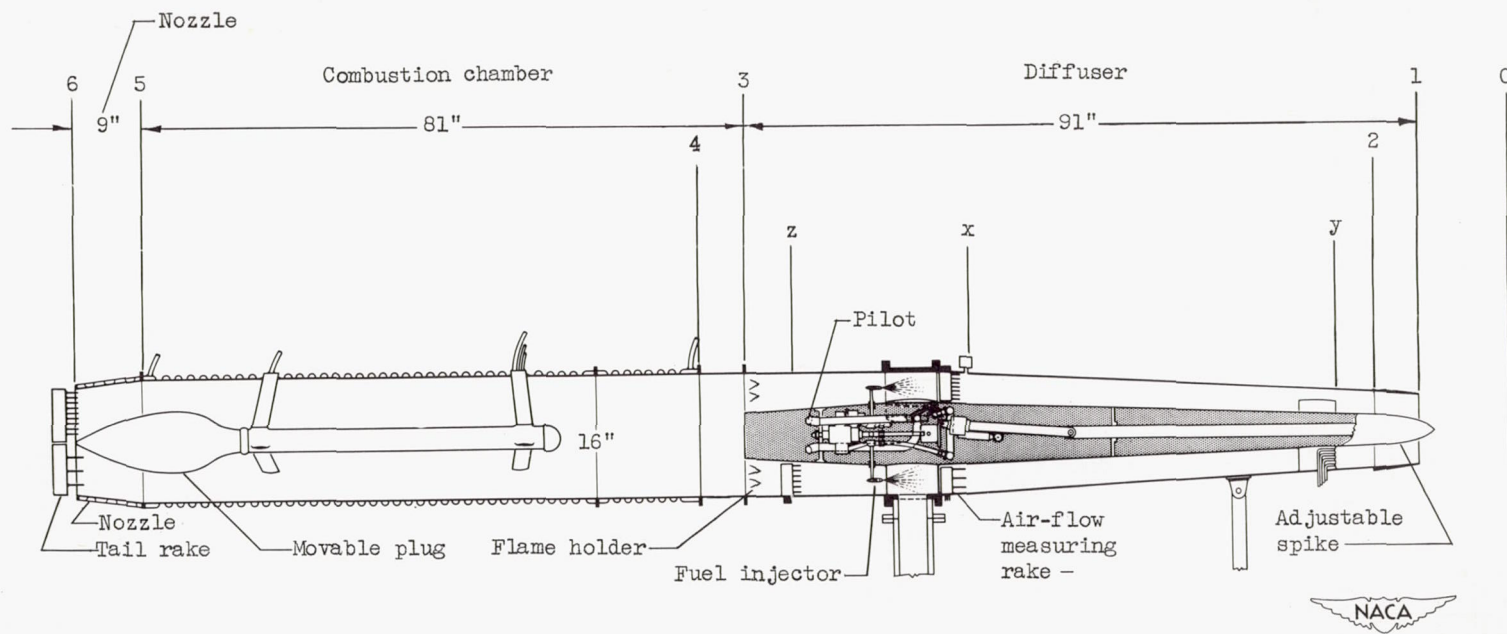


Figure 1. - Schematic diagram of 16-inch ram jet.



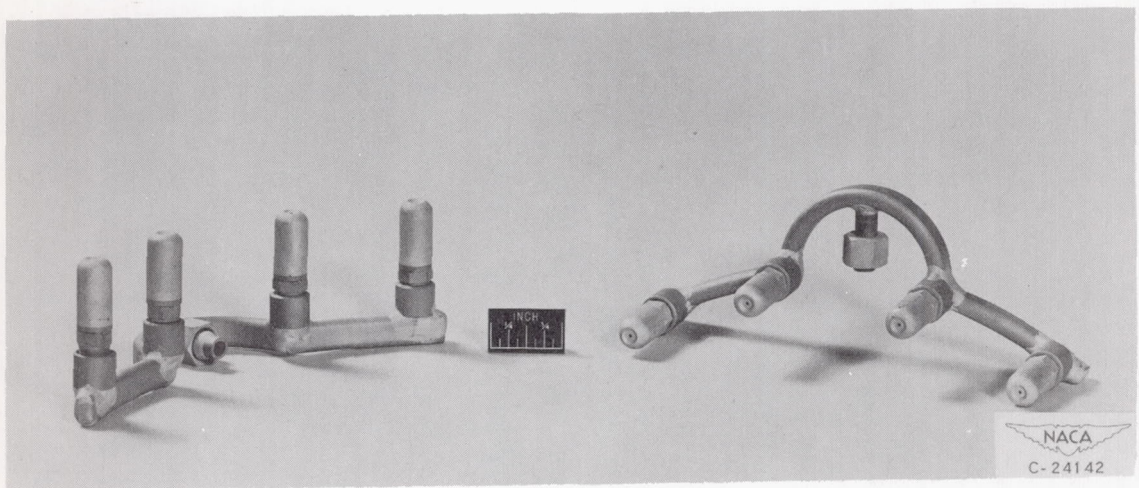
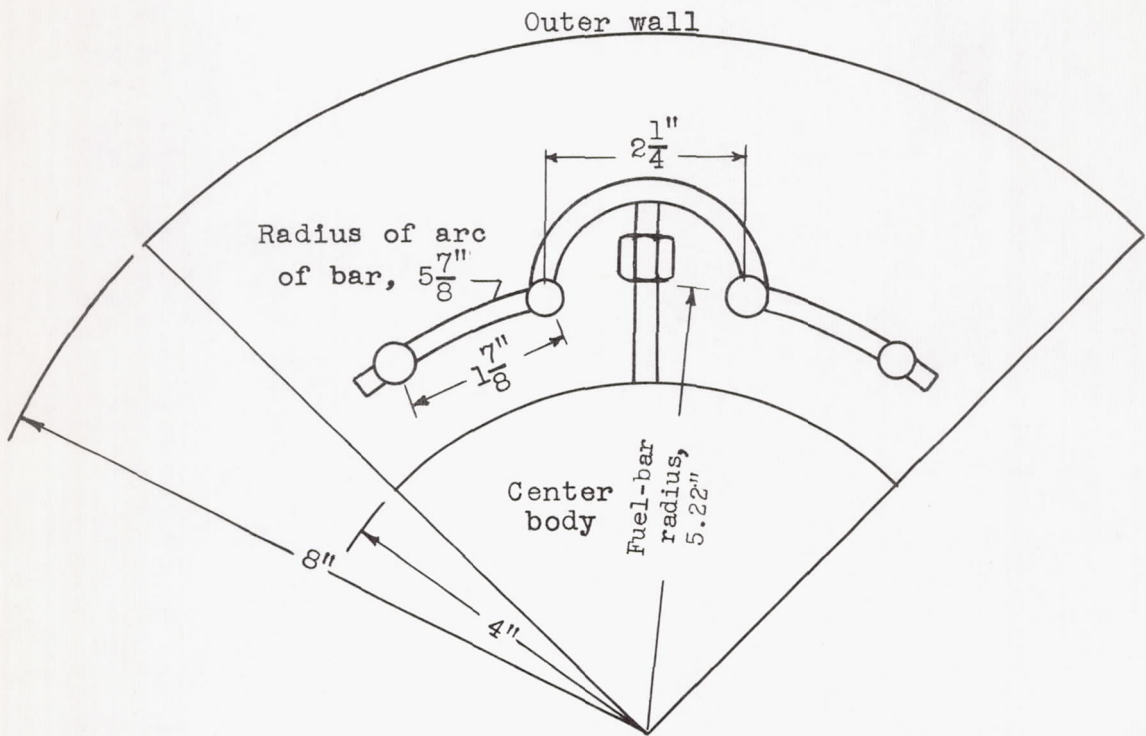
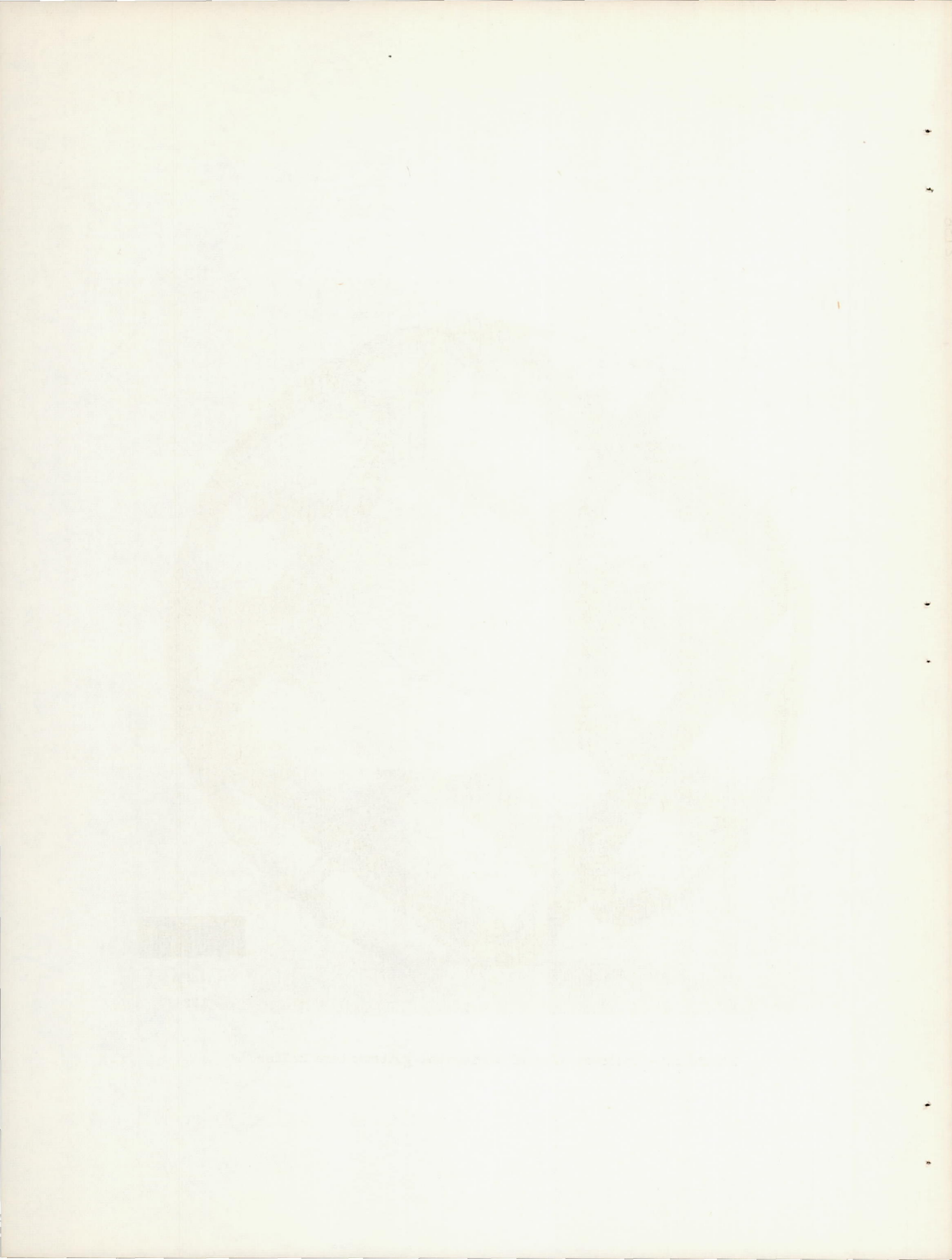


Figure 2. - Spray-nozzle fuel injector. (Nozzles rated at 0.347 gal/min at 100 lb/sq in.)



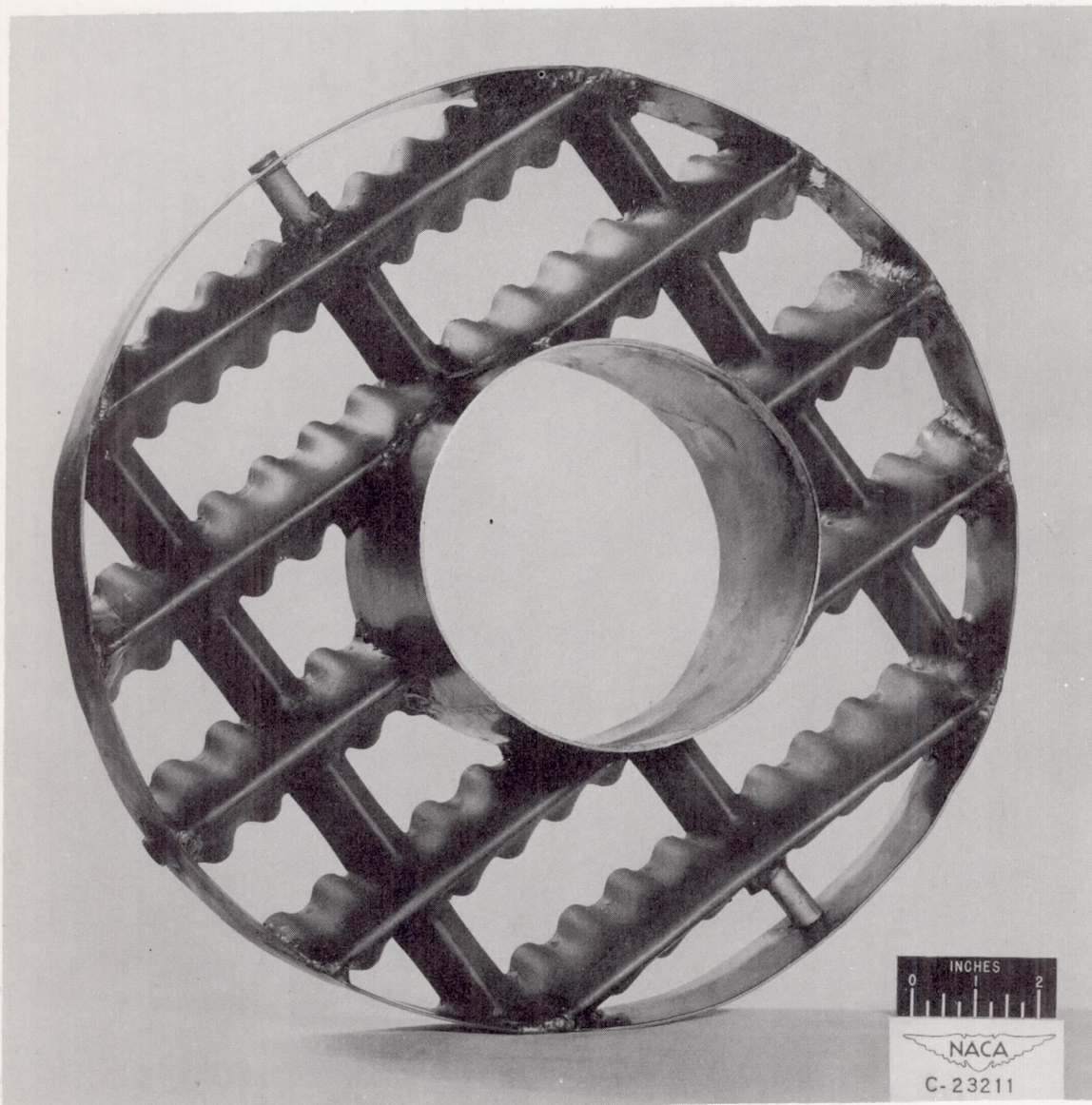
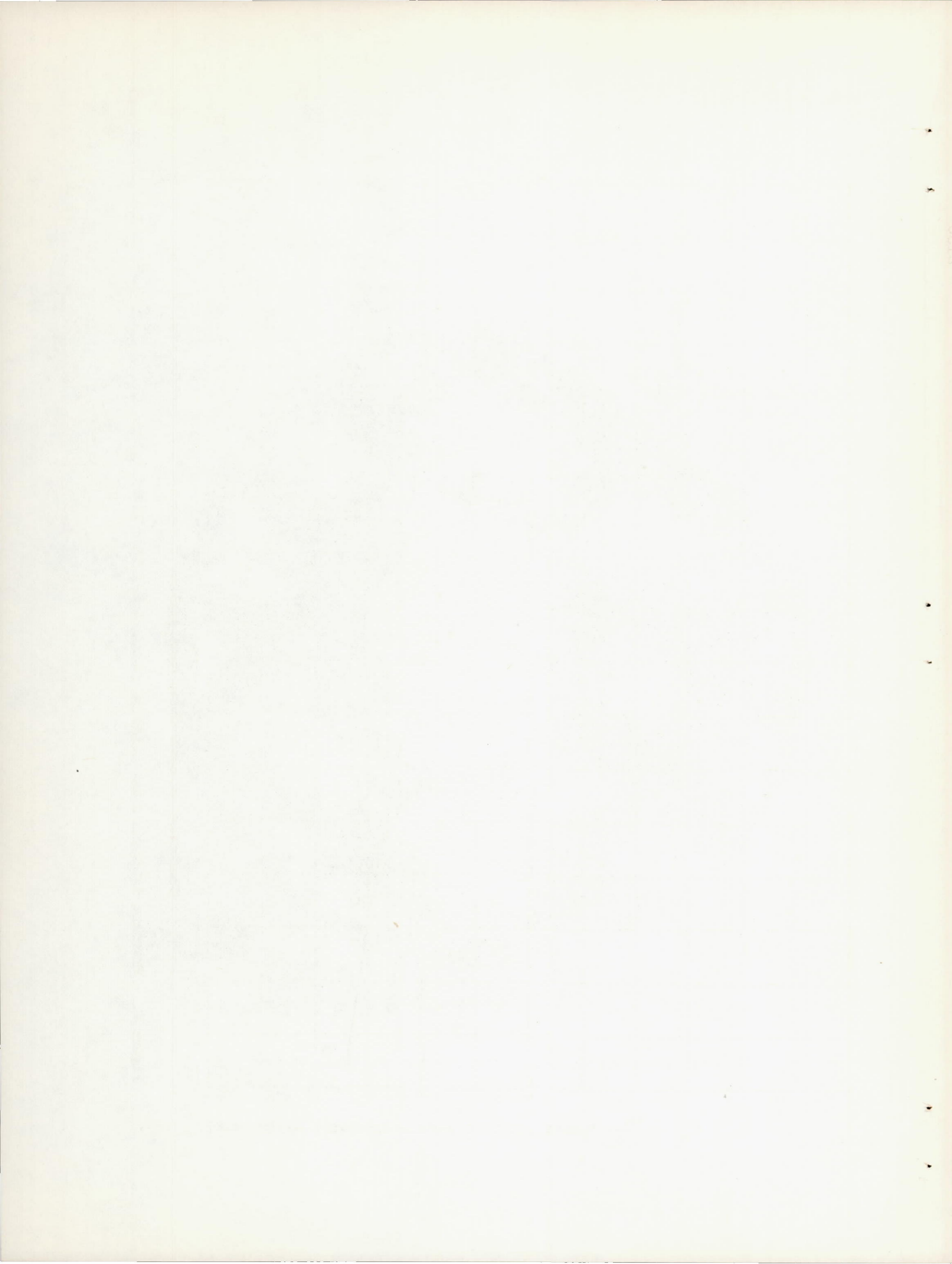


Figure 3. - Upstream view of corrugated-gutter flame holder.



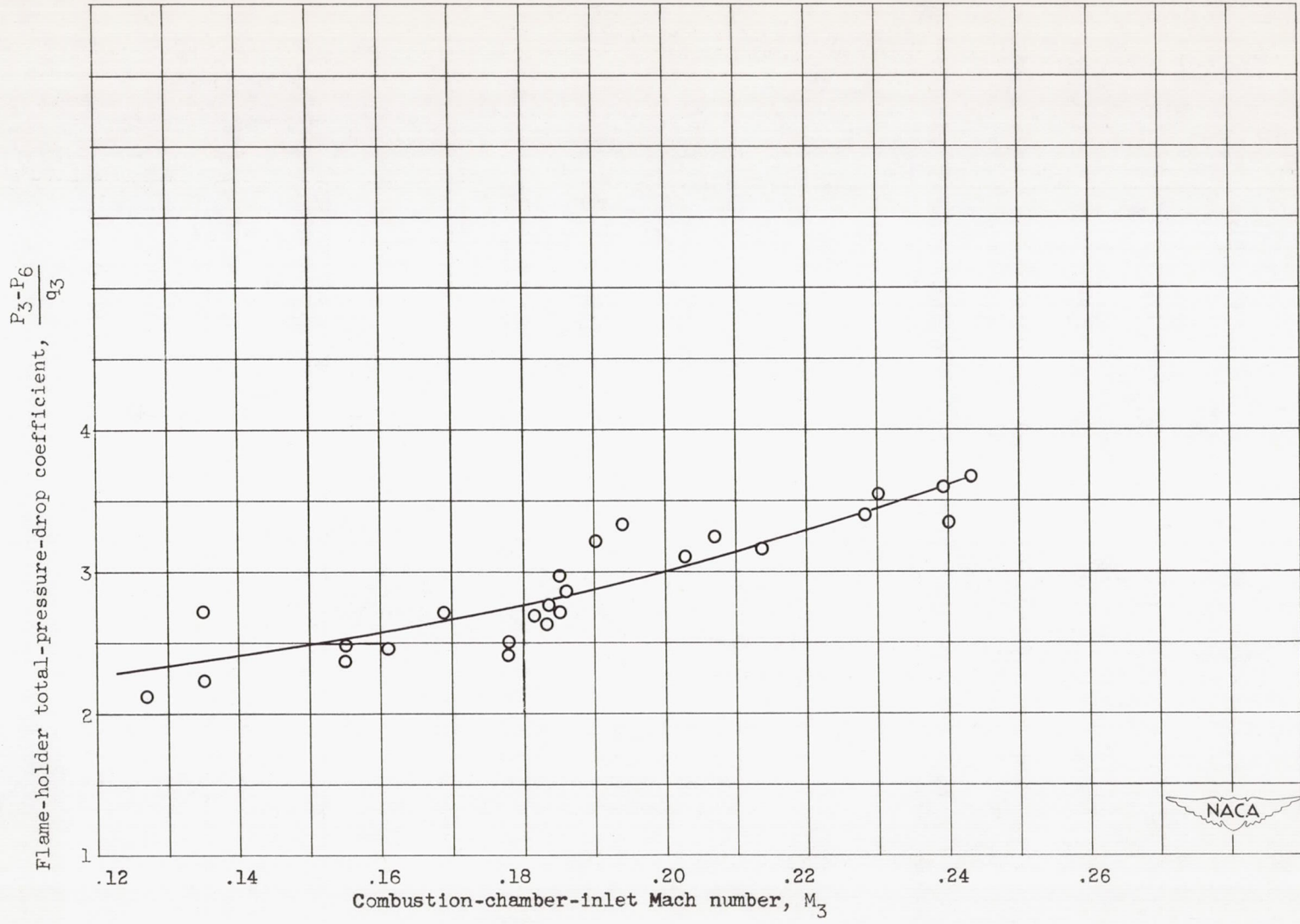


Figure 4. - Pressure-drop characteristics of corrugated-gutter flame holder.

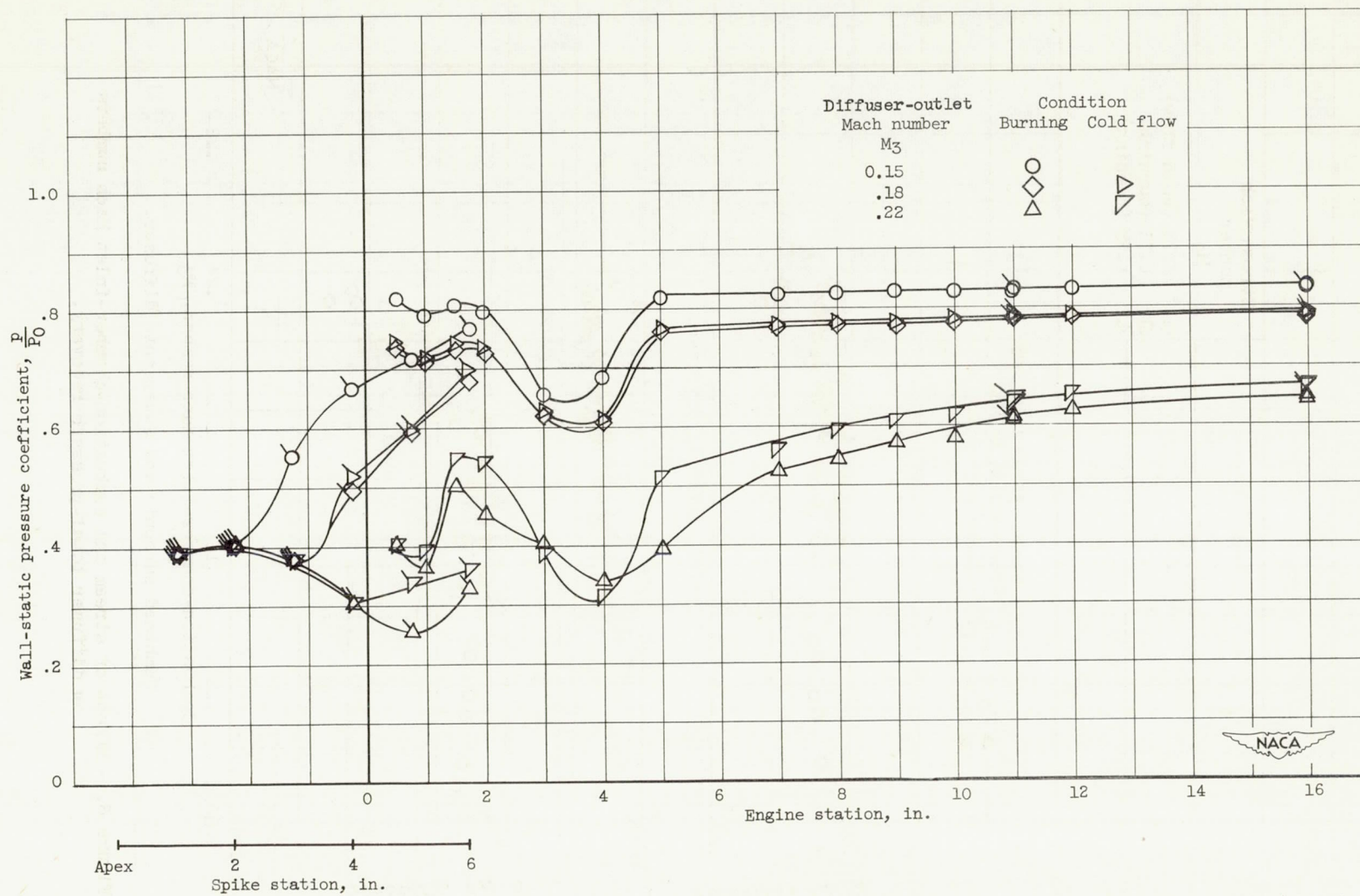


Figure 5. - Effect of diffuser-outlet Mach number on wall-static-pressure distribution in region of diffuser inlet.  $M_0 = 1.73$ . (Tailed symbols denote spike or inner-body readings.)

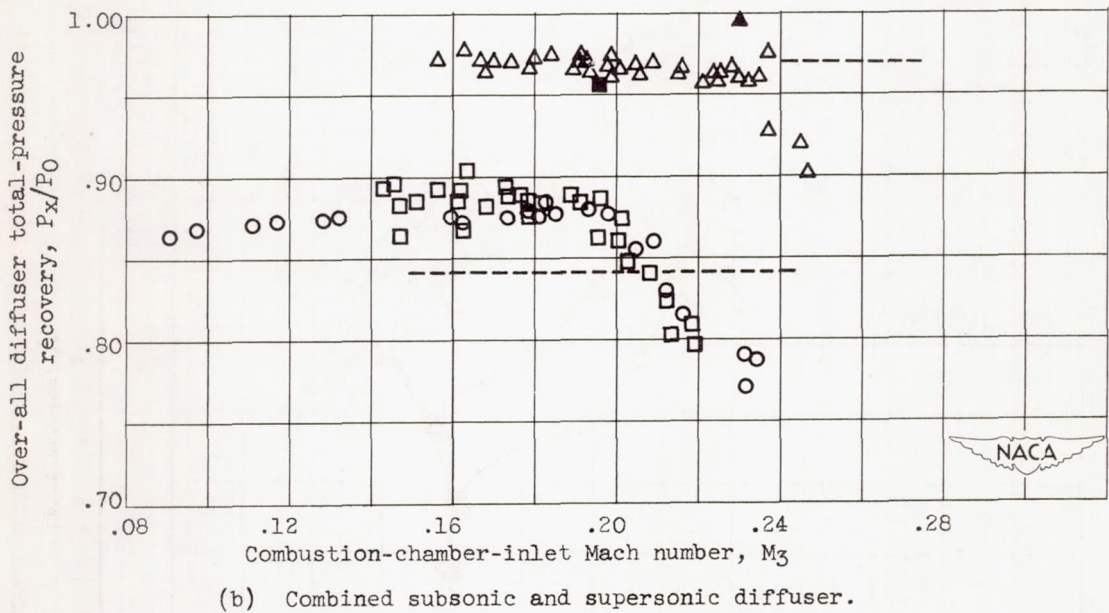
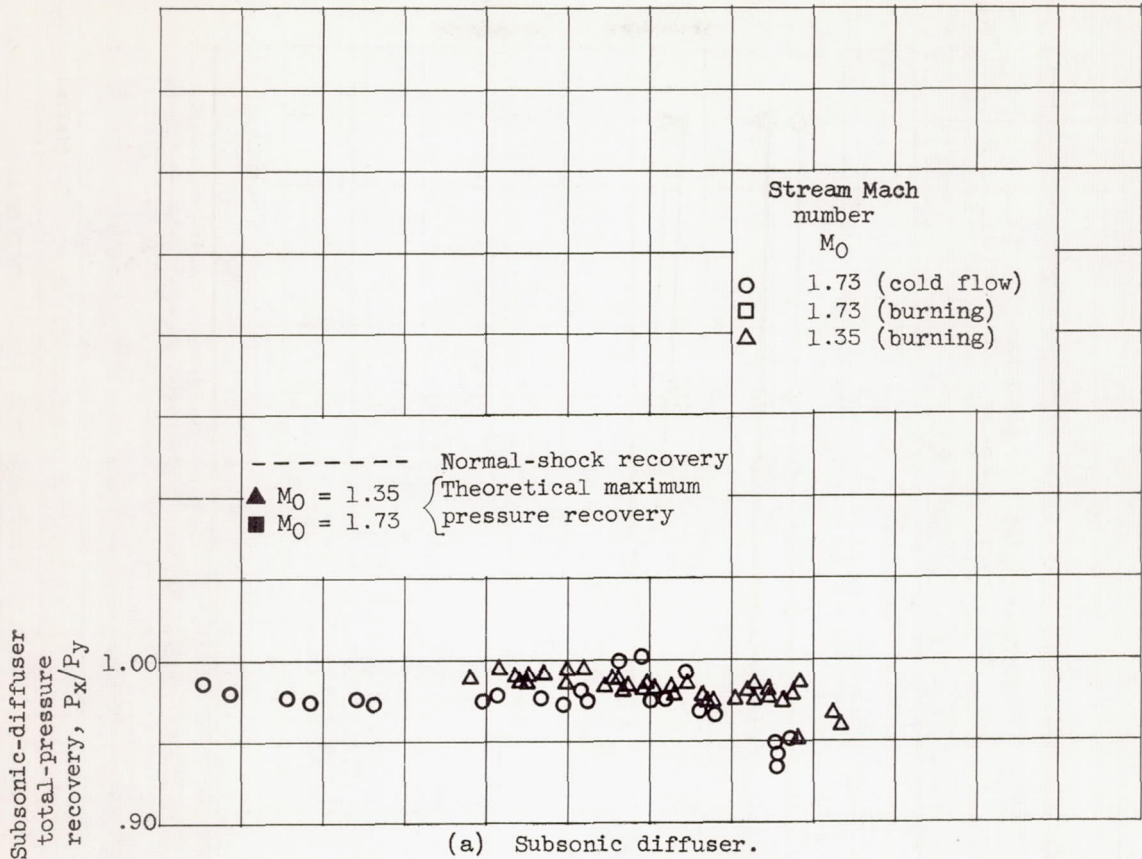


Figure 6. - Effect of stream and combustion-chamber-inlet Mach numbers on diffuser total-pressure recovery.



2136

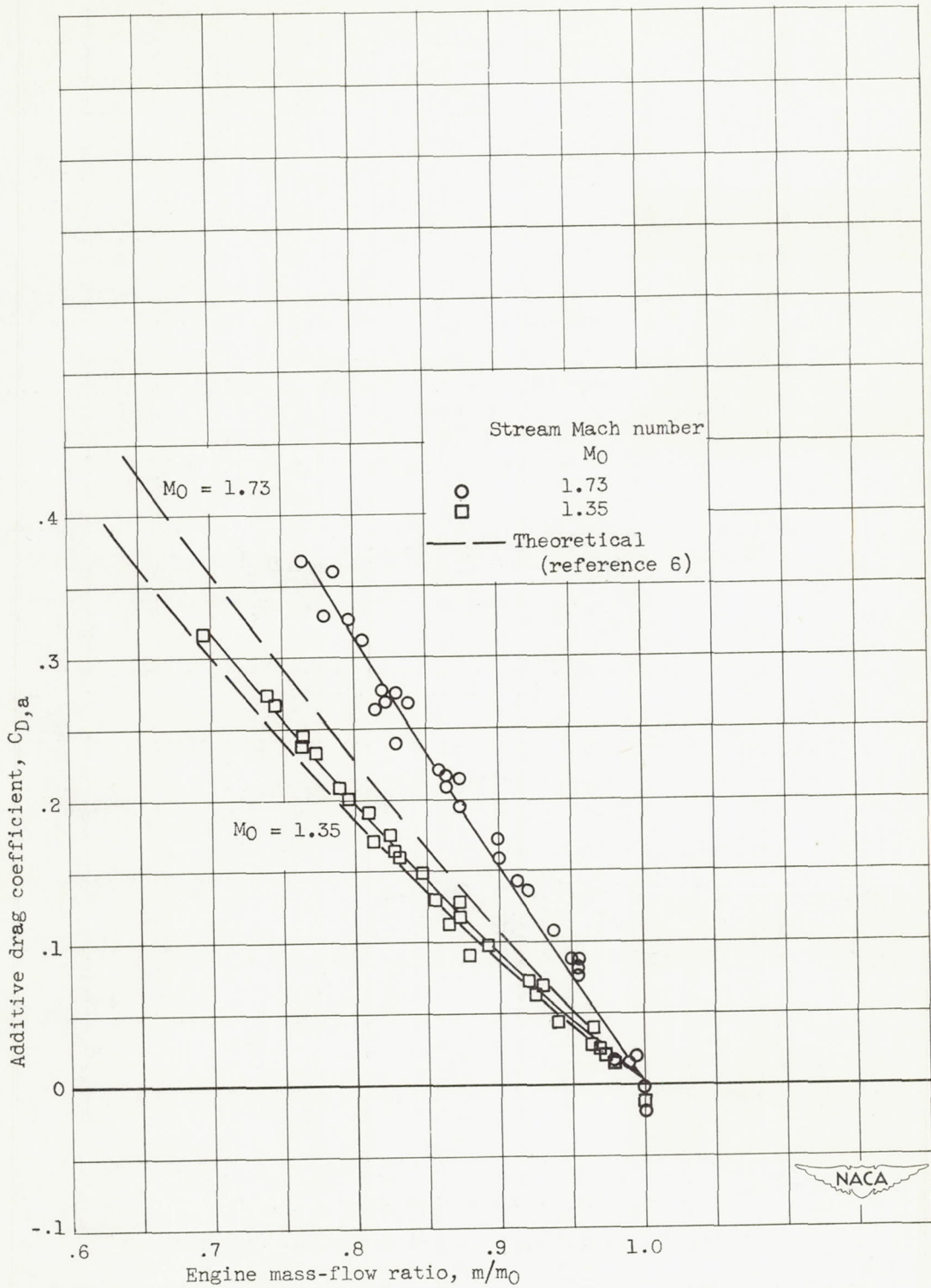
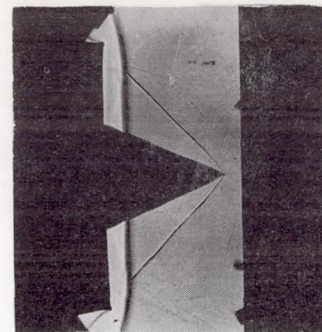
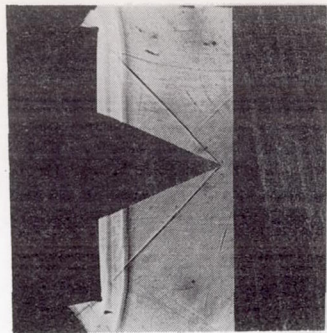
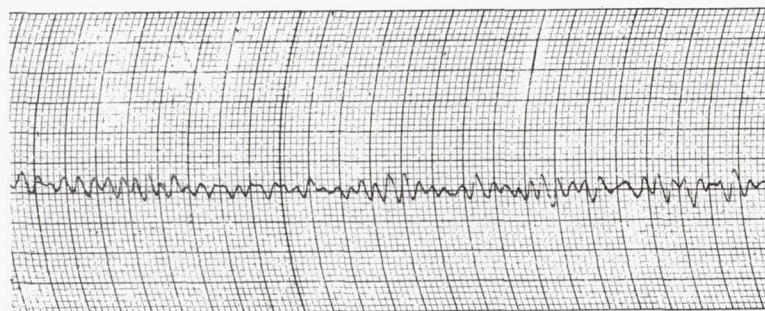


Figure 7. - Effect of mass-flow ratio and Mach number on additive drag coefficient. ( $C_{D,a}$  based on diffuser-inlet area.)



NACA  
C-27379



$\Delta P = \pm 0.31$  pounds per square inch

(a) Burning conditions.



$\Delta P = \pm 0.13$  pounds per square inch

(b) Cold-flow conditions.

Figure 8. - Comparison between diffuser shock stability and internal static-pressure fluctuations under cold-flow and burning conditions.  $M_0 = 1.73$ ;  $M_3 = 0.17$ .



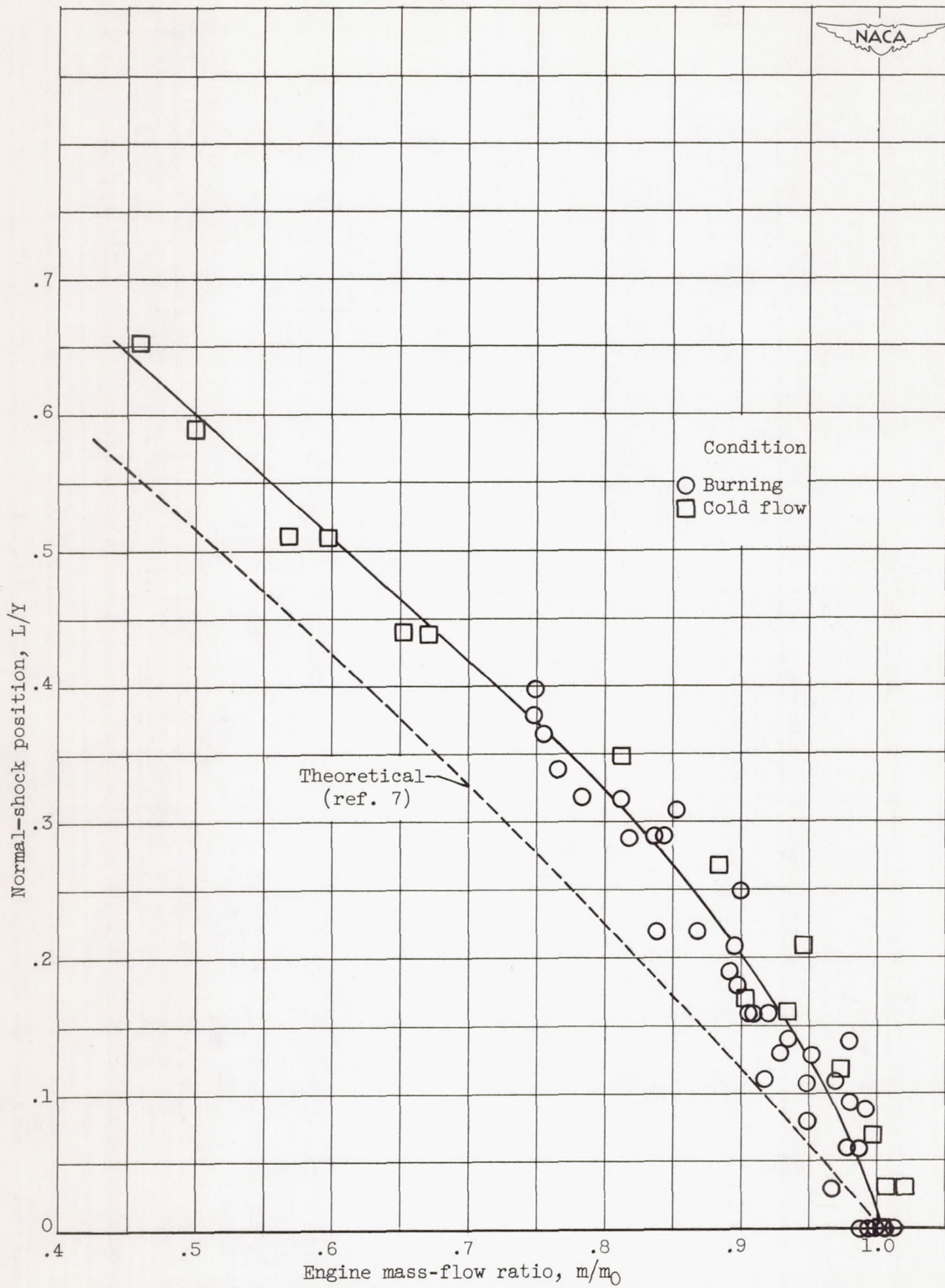


Figure 9. - Relation between engine air flow and normal-shock position for  $M_0 = 1.73$ .

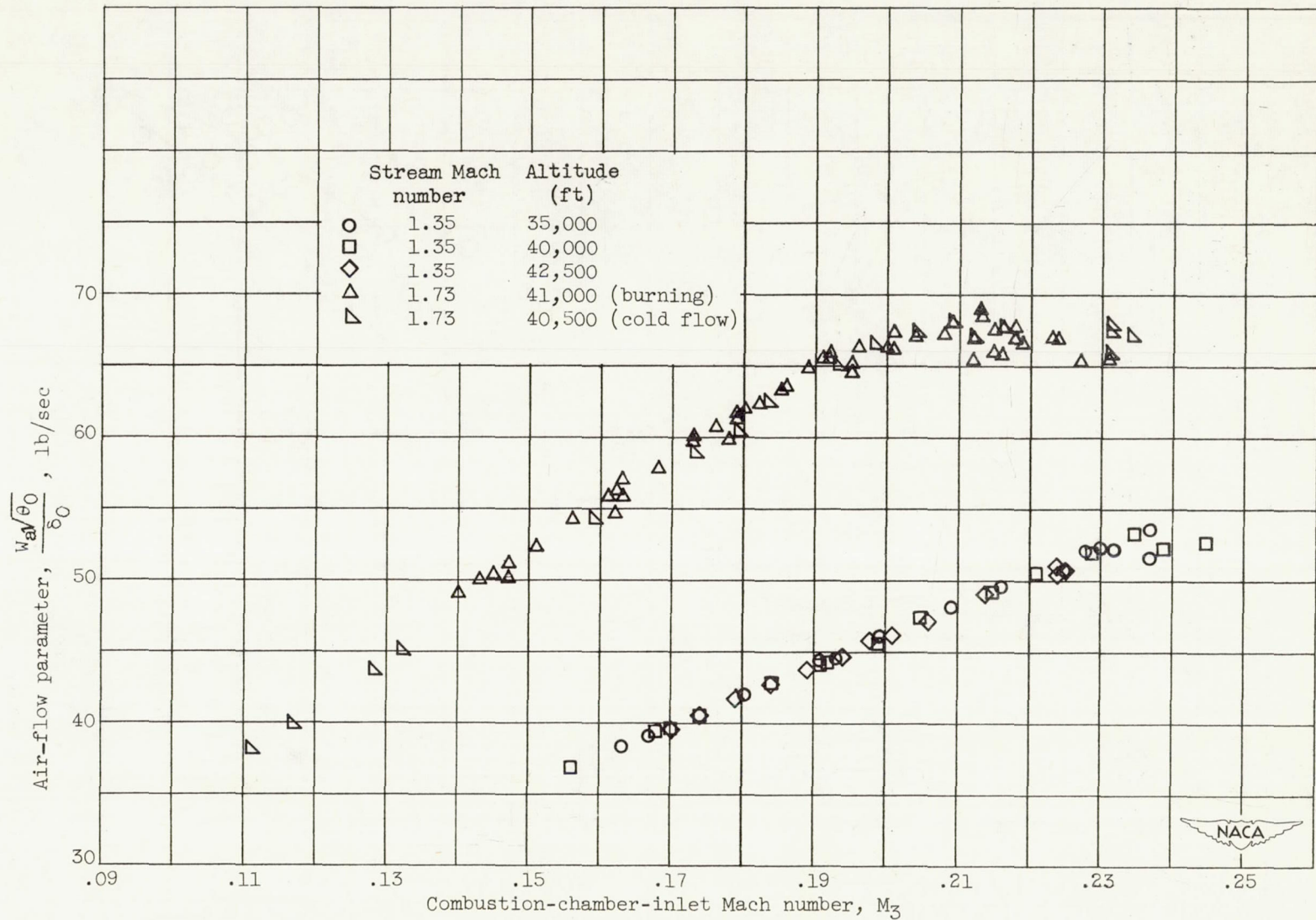
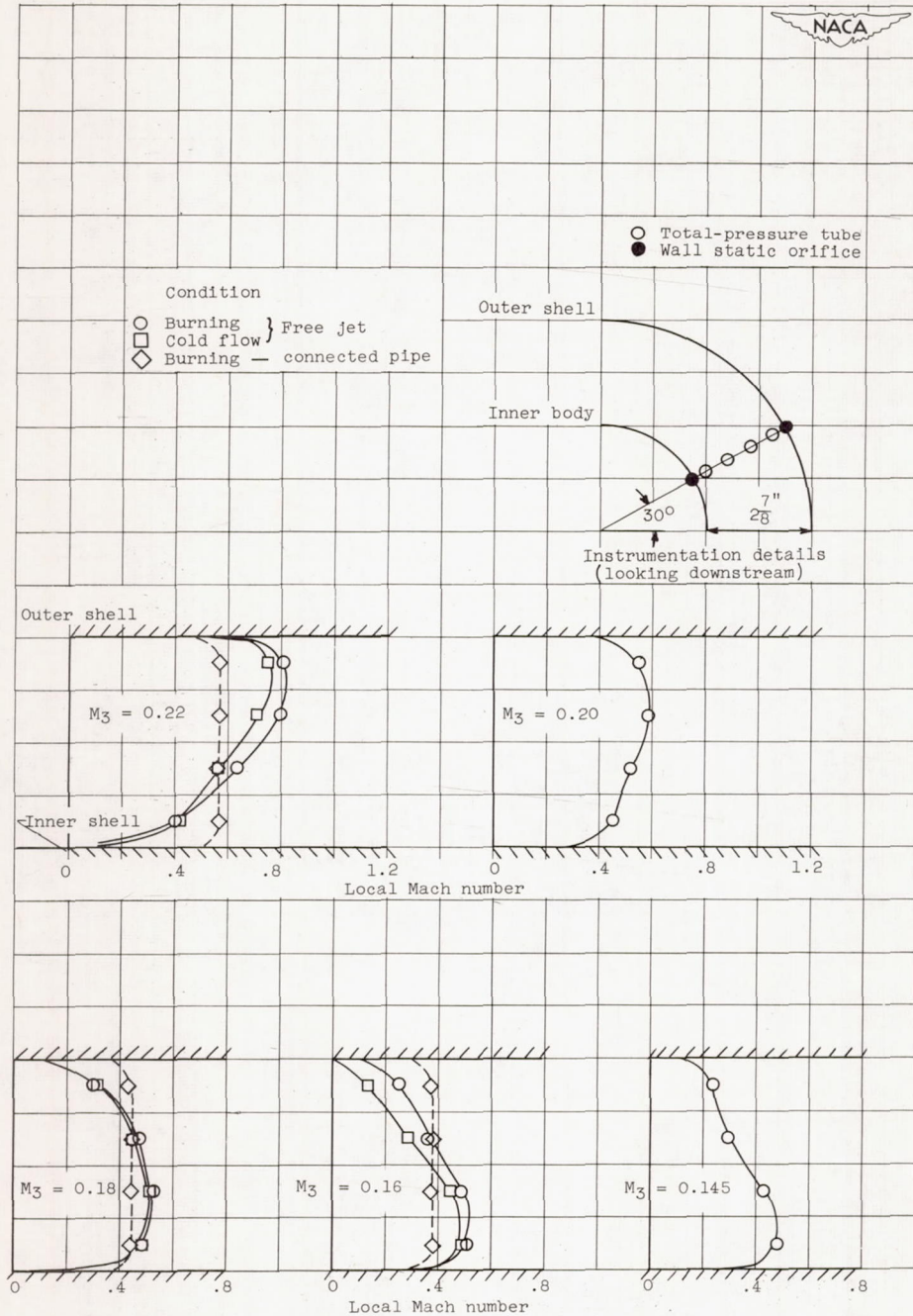
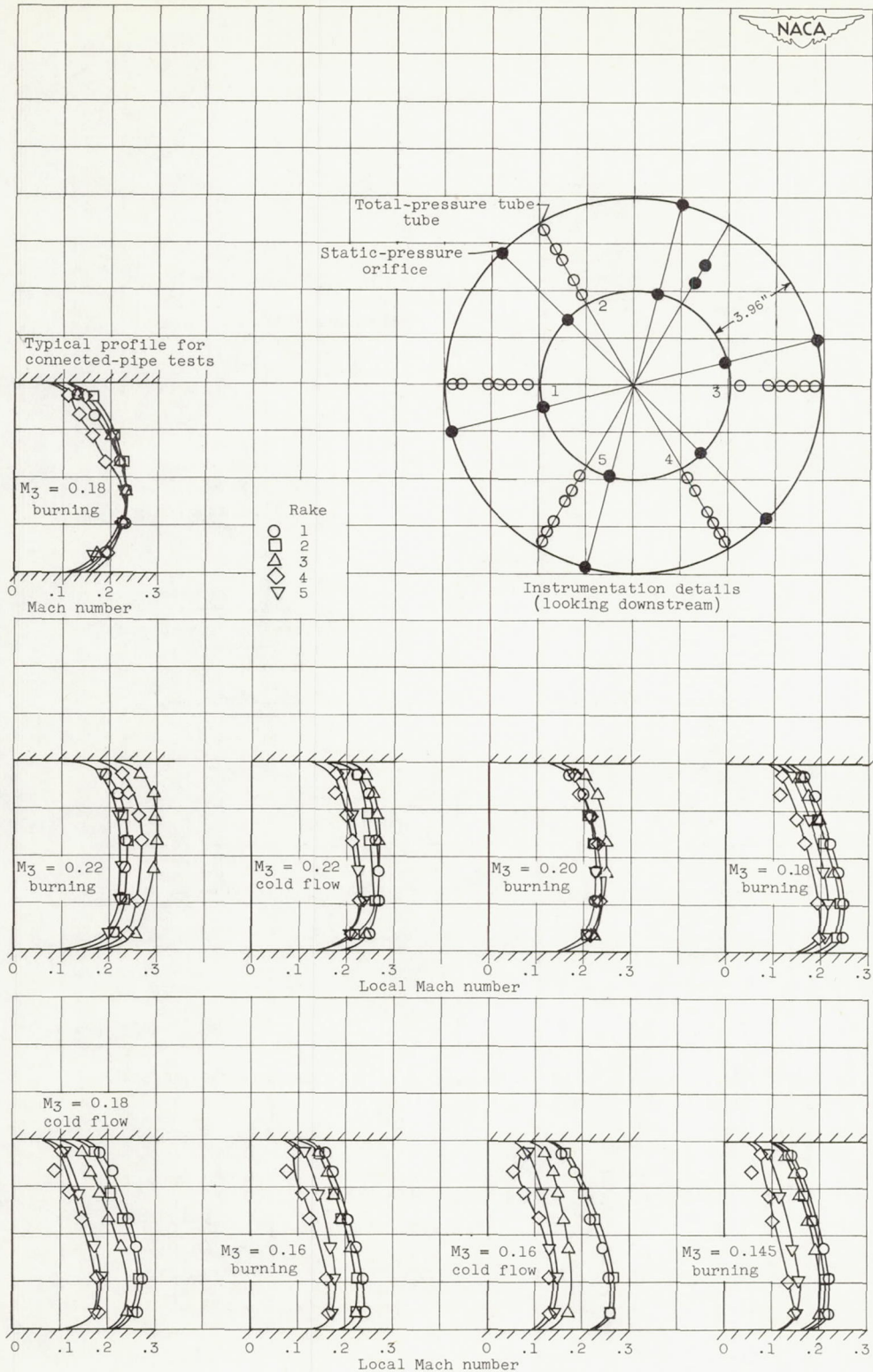


Figure 10. - Variation of air-flow parameter with stream and combustion-chamber-inlet Mach number.



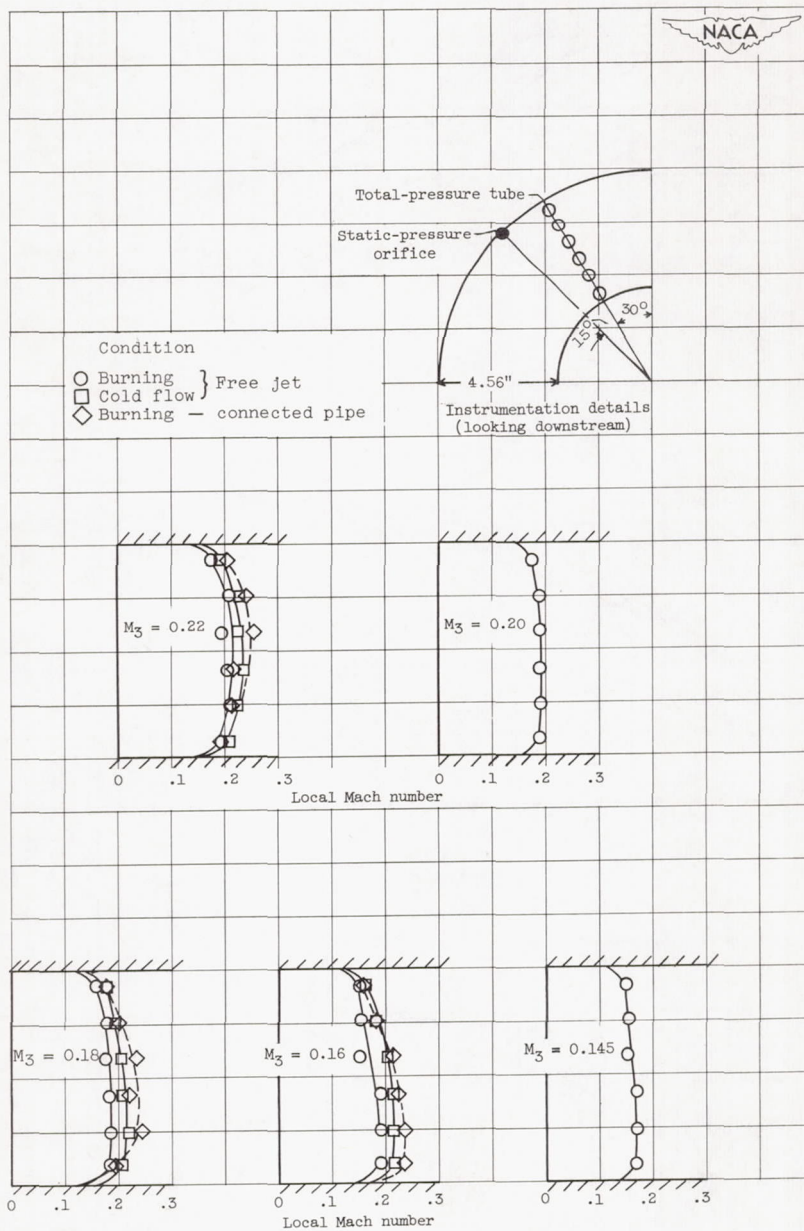
(a) Station y, 12 inches from inlet lip.

Figure 11. - Effect of combustion-chamber-inlet Mach number on velocity distribution at selected diffuser stations.  $M_0 = 1.73$ .



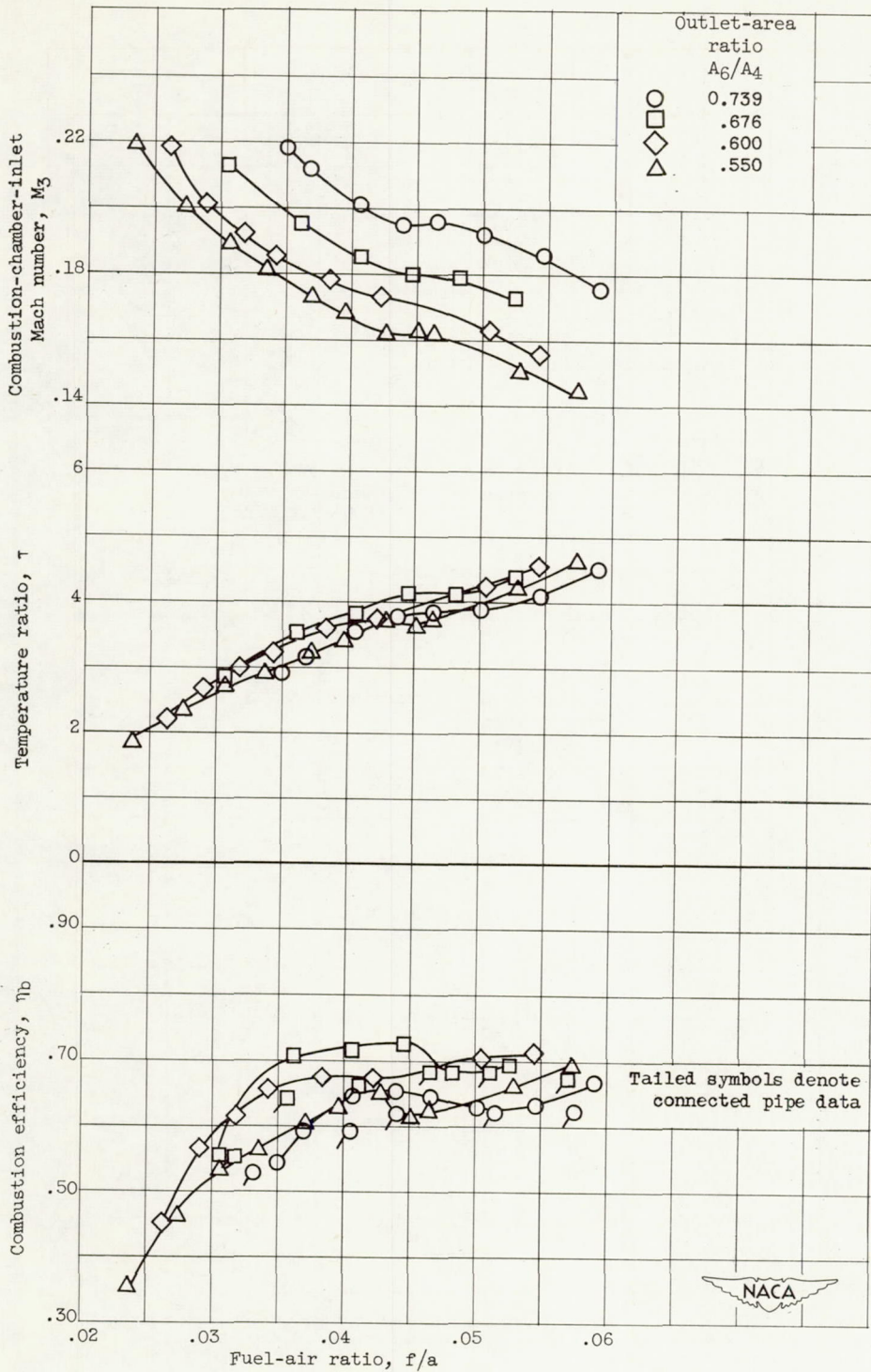
(b) Station x, 62 inches from inlet lip.

Figure 11. - Continued. Effect of combustion-chamber-inlet Mach number on velocity distribution at selected diffuser stations.  $M_0 = 1.73$ .



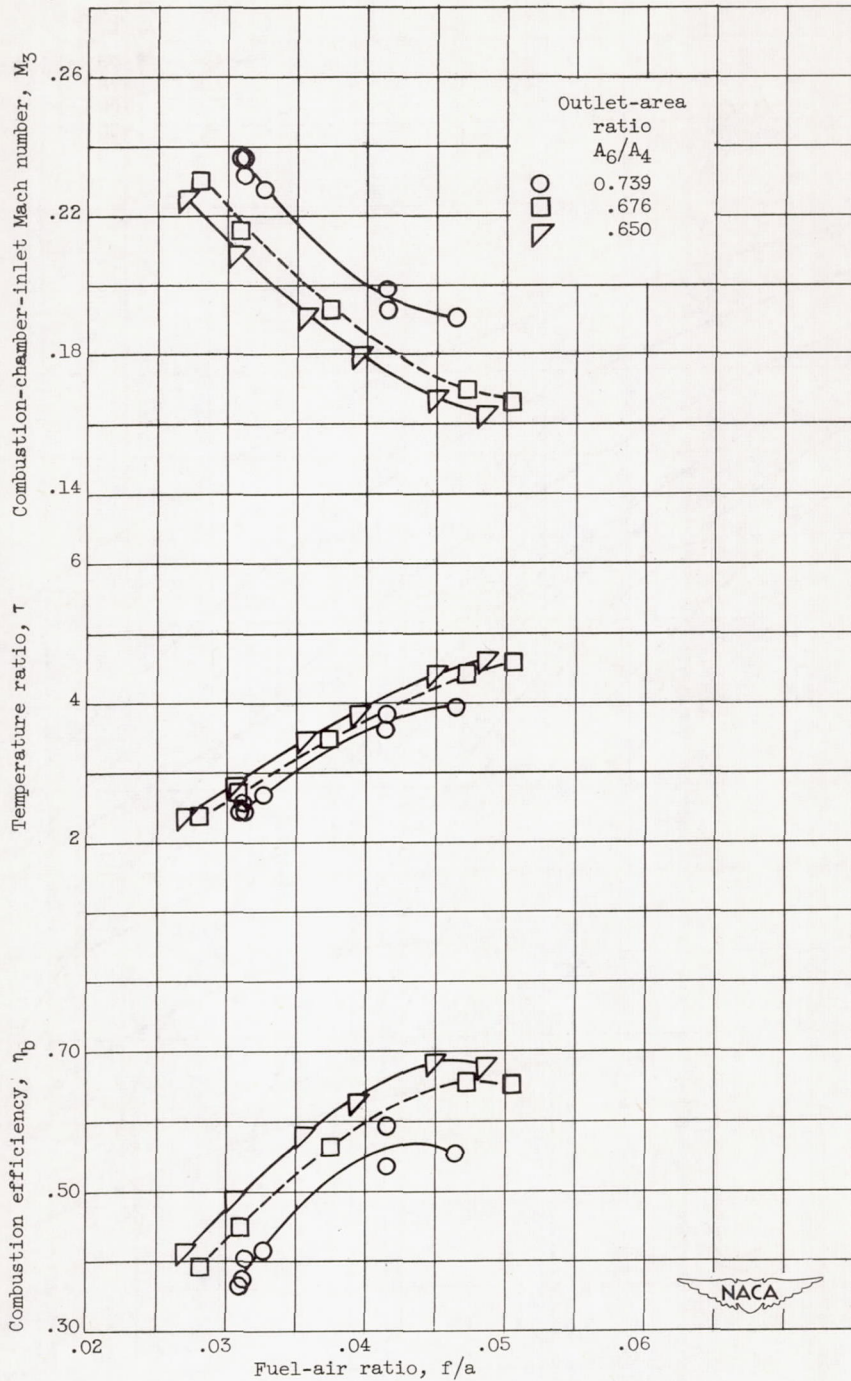
(c) Station z, 84 inches from inlet lip.

Figure 11. - Concluded. Effect of combustion-chamber-inlet Mach number on velocity distribution at selected diffuser stations.  $M_0 = 1.73$ .



(a)  $M_0 = 1.73$ ; altitude, 41,000 feet.

Figure 12. - Effect of fuel-air ratio and exhaust-nozzle area on combustion-chamber performance.



(b)  $M_0 = 1.35$ ; altitude, 35,000 feet.

Figure 12. - Concluded. Effect of fuel-air ratio and exhaust-nozzle area on combustion-chamber performance.

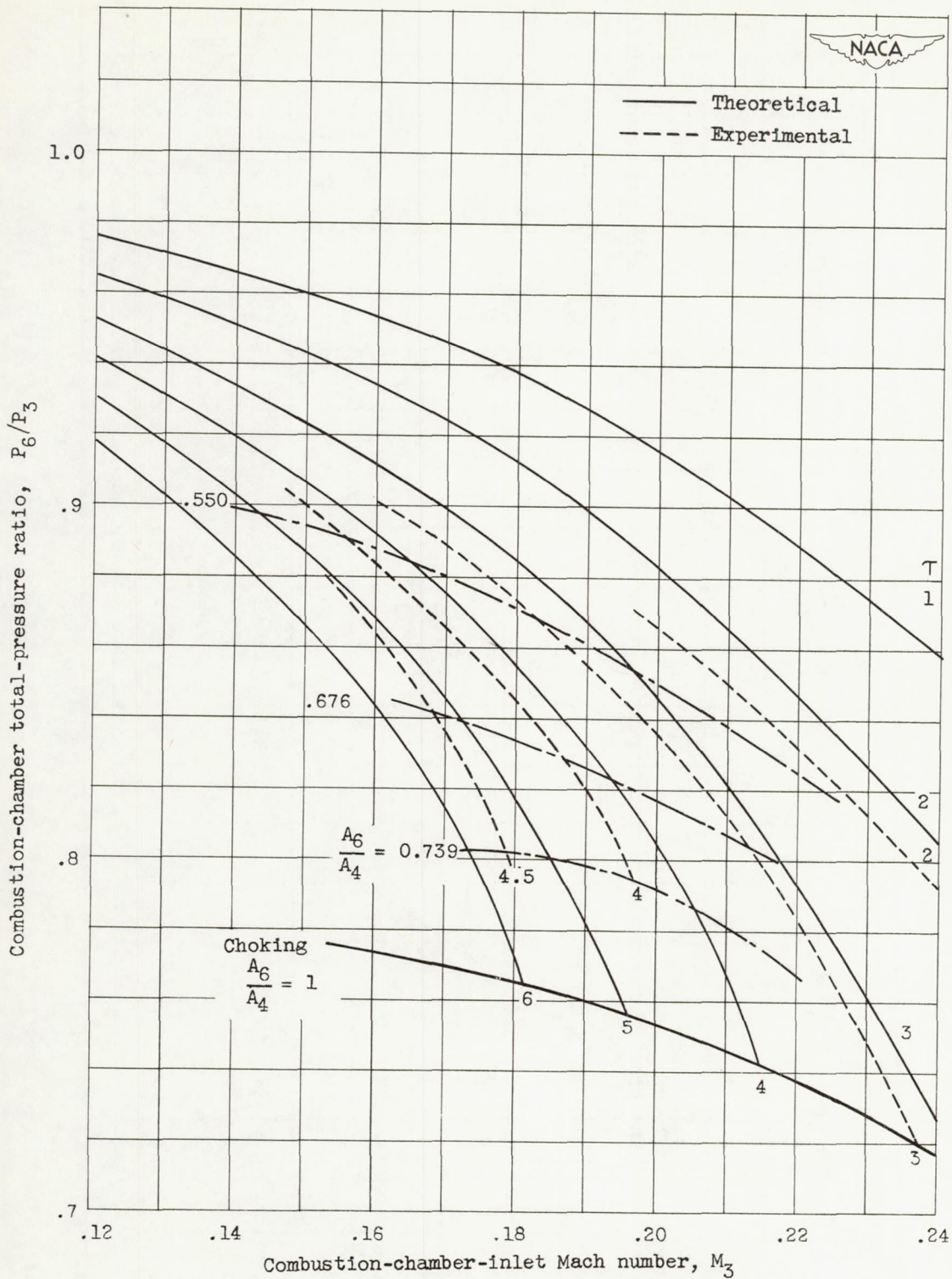
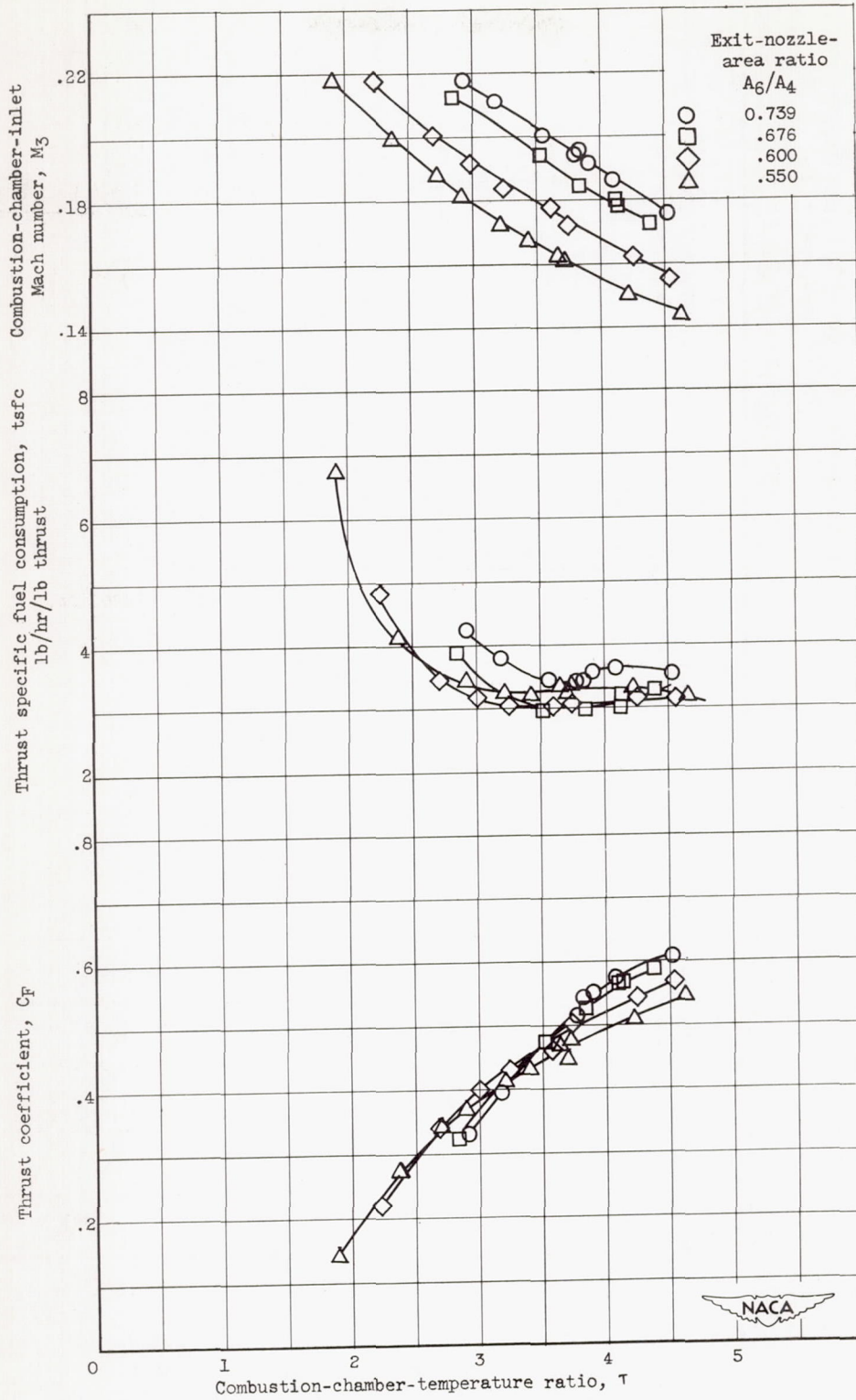
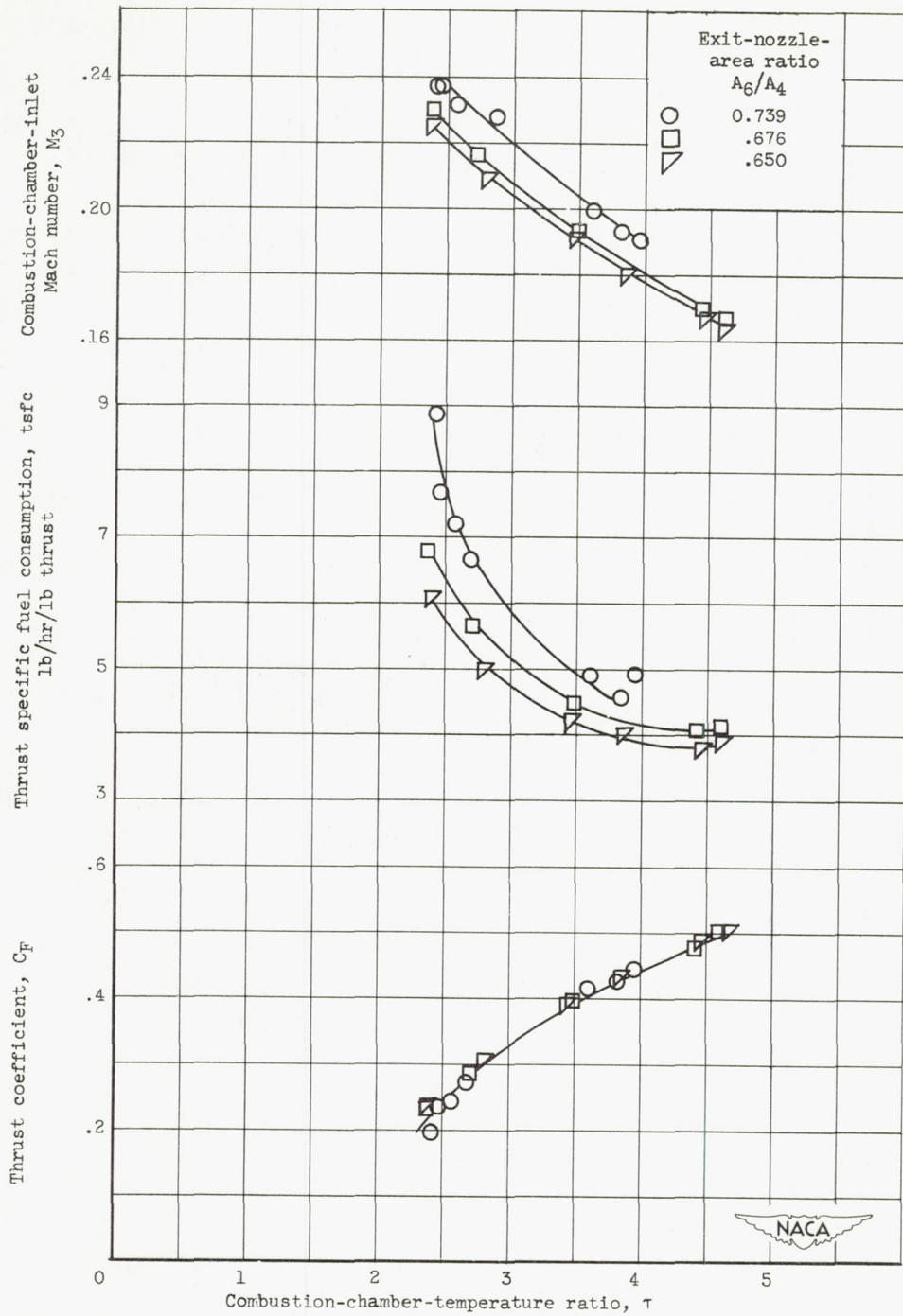


Figure 13. - Effect of inlet Mach number and combustion-chamber-temperature ratio on combustion-chamber total-pressure losses (including flame holder).



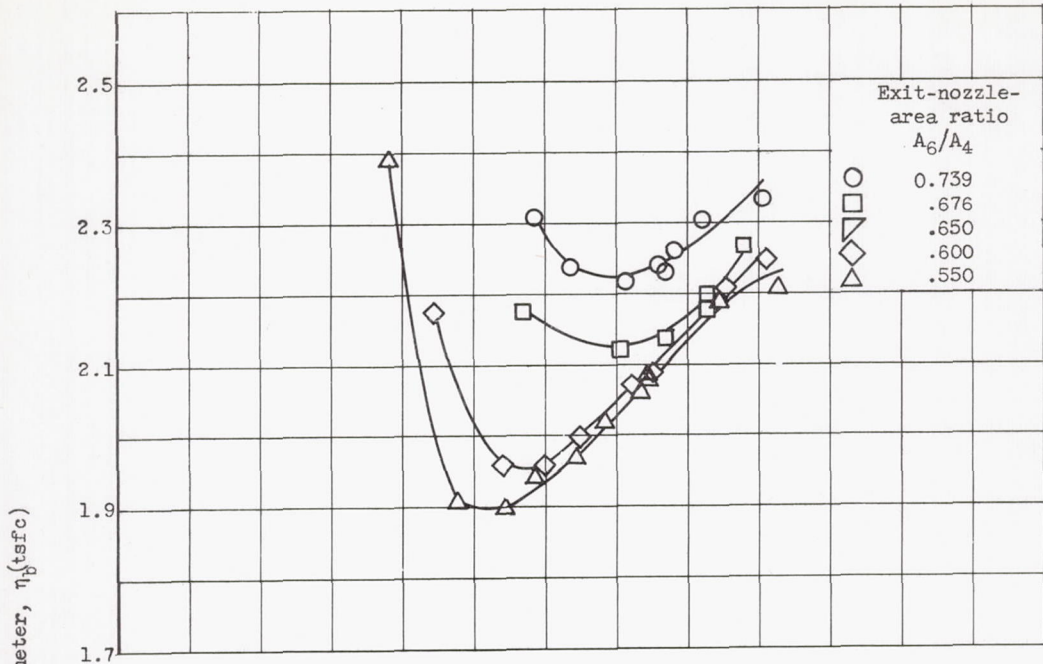
(a)  $M_0 = 1.73$ ; altitude, 41,000 feet.

Figure 14. - Effect of combustion-chamber-temperature ratio and exit-nozzle area on engine performance.

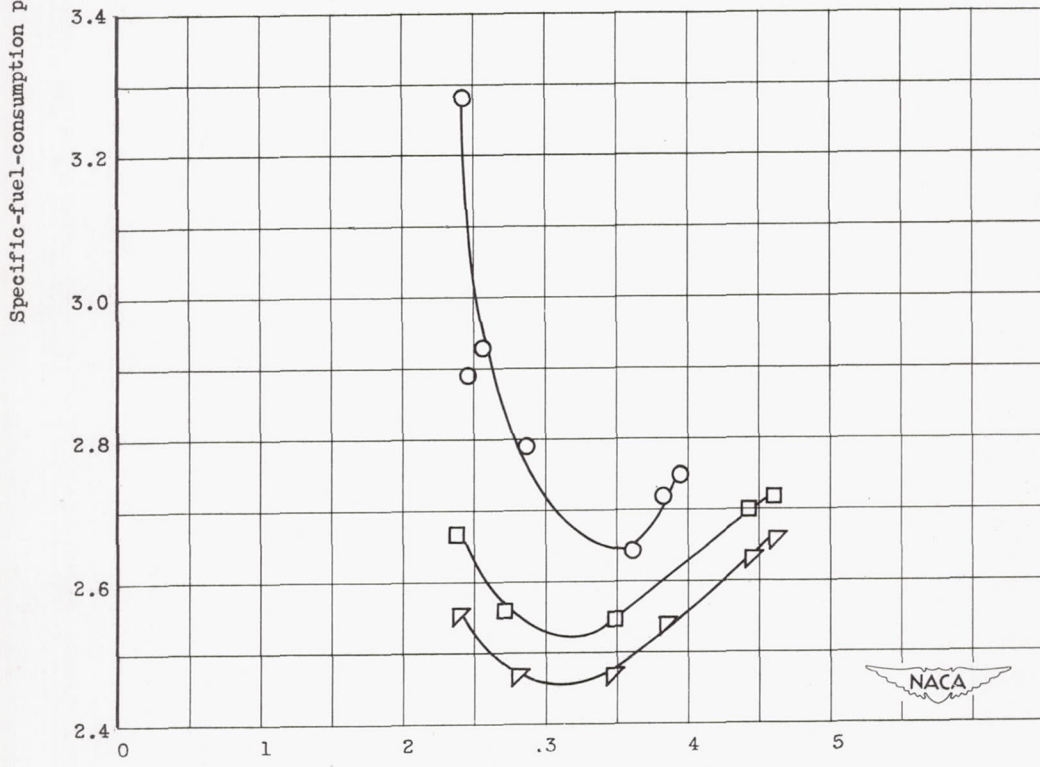


(b)  $M_0 = 1.35$ ; altitude, 35,000 feet.

Figure 14. - Concluded. Effect of combustion-chamber-temperature ratio and exit-nozzle area on engine performance.



(a)  $M_0 = 1.73$ ; altitude, 41,000 ft.



(b)  $M_0 = 1.35$ ; altitude, 35,000 ft.

Figure 15. - Effect of combustion-chamber-temperature ratio and exit-nozzle area on fuel-consumption parameter.

